symmetry

MDPI

Article

Neutrinoless Double-Beta Decay Investigations of ^{82}Se Using Three Shell Model Hamiltonians

Andrei Neacsu [1,2,*] and Mihai Horoi [3]

[1] International Center for Advanced Training and Research in Physics (CIFRA), 077125 Magurele, Romania
[2] Horia Hulubei National Institute for R&D in Physics and Nuclear Engineering (IFIN-HH), 077125 Magurele, Romania
[3] Department of Physics, Central Michigan University (CMU), Mount Pleasant, MI 48859, USA; mihai.horoi@cmich.edu
* Correspondence: neandrei@gmail.com

Abstract: Neutrinoless double-beta decay is considered one of the most promising processes that would help clarify some of the symmetry-breaking problems in our understanding of the observable universe. Recent studies of neutrinoless double-beta decay matrix elements have employed statistical approaches based on modified shell model effective Hamiltonians for ^{48}Ca (Phys. Rev. C 106, 054302 (2022)) and ^{136}Xe (Phys. Rev. C 107, 045501 (2023)). The analyses rely on inducing perturbations in the starting effective Hamiltonians to observe the behavior of a wide range of observables, besides the $0\nu\beta\beta$) NME, that are compared with experimental data. Following a Bayesian model averaging approach, the range of probable values for the neutrinoless double-beta decay matrix elements is presented. In this paper, we present a similar study for ^{82}Se, which is described in the same model space as ^{76}Ge that is under experimental observation. Due to its faster calculation time compared to ^{76}Ge, ^{82}Se can be used as an appropriate substitute in our complex statistical study. Using the calculations performed for the statistical analysis of the neutrinoless double-beta decay matrix elements, we also search for the correlations between the observables that we can compare to experimental data.

Keywords: shell model; double beta decay; nuclear matrix elements; statistical analysis

Citation: Neacsu, A.; Horoi, M. Neutrinoless Double-Beta Decay Investigations of ^{82}Se Using Three Shell Model Hamiltonians. *Symmetry* **2024**, *16*, 974. https://doi.org/10.3390/sym16080974

Academic Editor: Abraham A. Ungar

Received: 14 June 2024
Revised: 19 July 2024
Accepted: 22 July 2024
Published: 31 July 2024

1. Introduction

Our currently accepted model of the laws governing the nuclear structure, nuclear reactions, elementary particles, and fundamental fields, called the Standard Model, requires in its current formulation the conservation of the lepton number and the lepton flavor. The experimental confirmation of neutrino oscillations [1,2], which were predicted by theoretical models a few decades before [3,4], has demonstrated that lepton flavor is not a fundamental symmetry. The significance of this discovery was recognized with the Nobel Prize in 2015 [5]. In beta decay ($\beta^{-/+}$), an electron/positron is emitted from a nucleus. Thus, an accompanying (anti)neutrino needs to emerge, to satisfy the symmetry that is required to balance out the production of leptons and antileptons in this transition. On a fundamental level, the symmetry between particles and anti-particles that can be generated has been verified experimentally with high precision, but this poses a problem for our understanding of the observed universe composed mostly of matter, with antimatter being found in insignificant amounts and for very a brief time, like in the case of positrons emitted from β^+ reactions, that quickly annihilate with surrounding electrons which are abundant. To solve this so-called "asymmetry problem", many theories have been proposed over the last decades that aim to extend the standard model, including the prediction of processes that can violate some of its fundamental symmetries. Experiments are dedicated to the study of such symmetry-breaking processes, such as the MAJORANA Collaboration, aiming at charge non-conservation and Pauli exclusion principle violation [6].

The neutrinoless double-beta ($0\nu\beta\beta$) decay is a yet unobserved nuclear process competing with the known two-neutrino double-beta transition that was observed for 11 isotopes [7], but with the emission of only two electrons sharing the entire energy, not accompanied by their respective antineutrinos. This decay violates lepton number conservation by two units, making it a unique and interesting phenomenon in nuclear and particle physics [8]. The observation of $0\nu\beta\beta$ decay would provide strong evidence for new physics beyond the Standard Model (BSM) and support the existence of Majorana neutrinos. The implications of such a discovery could reveal many of the unknown properties of neutrinos [9,10] and would provide a path to the extension of the SM Lagrangian [11,12]. Theoretical models suggest that if Majorana neutrinos exist and neutrino masses originate from a type of seesaw mechanism called Type I or Type II seesaw, then neutrinoless double-beta decay should occur naturally. The detection of $0\nu\beta\beta$ decay could also indicate the existence of right-handed currents, which would suggest that right-handed neutrino currents play a role in mediating weak interactions, as it is predicted in the left–right symmetric model [13]. If neutrinoless double beta decay was observed, then this could also have implications on other areas such as dark matter searches or even grand unified theories (GUTs). For example, GUT models often predict new particles beyond those already known from experiments at CERN's Large Hadron Collider; however, these predictions are usually very difficult to test experimentally due to their high energies involved. The possibility of neutrinoless double-beta decay would open a path for us to study these predictions at low energies. The results from ongoing experiments provide increasingly stringent limits on the rate at which $0\nu\beta\beta$ decay might occur, helping to narrow down theoretical models for its non-observation. The search for $0\nu\beta\beta$ decay continues with collaborative efforts worldwide [14–17], using larger and more sensitive detectors in hopes of finally confirming or refuting this enigmatic phenomenon. So far, the most stringent results come from ^{76}Ge [14] and ^{136}Xe [17] with half-life limits of the order of $2 \cdot 10^{26}$ years.

In the case of the light left-handed Majorana neutrino exchange scenario, theoretical studies of this process describe the decay rate as a product of leptonic phase-space factors (PSF) of the outgoing electrons, nuclear matrix elements (NME) that depend on the nuclear structure of the parent and the daughter nuclei, and a lepton number violating parameter (LNV) related to the effective Majorana neutrino mass [18–20]. Since the LNV values are expected to be extracted from an eventual experimental observation of the $0\nu\beta\beta$ decay and the PSF have been already calculated with reliable and very accurate methods employed for a wide variety of transitions [21–28], the greatest uncertainty remains from the values of the NME that are calculated with various nuclear structure methods, most commonly: the interacting shell model methods [29–39], the proton–neutron quasiparticle random phase approximation (pn-QRPA) methods [20,40–45], the interacting boson approximation (IBA) methods [46,47], the energy density functional method [48], the projected Hartree Fock Bogoliobov (PHFB) method [49], the coupled-cluster method (CC) [50], the in-medium generator coordinate method (IM-GCM) [51], and the valence-space in- medium similarity renormalization group method (VS-IMSRG) [52]. Each of these methods has its own advantages and disadvantages, mainly related to the difficulty of the numerical calculations, the amount of correlations considered, and harmonic oscillator shells that can be accessed. Since these methods all rely on various parameters and approximation, the results they provide span over wide ranges [53], and the consensus is difficult to reach, sometimes even within the confines of a specific model. Another recent review of the status of the theoretical studies of $0\nu\beta\beta$ decay, together with a Bayesian discovery probability of future experiments is found in Ref. [54].

Of the popular nuclear structure models listed, the interacting shell model (ISM) presents the most stable framework, without the need to adjust parameters, and with predictions from different groups using different effective Hamiltonians that encode the nucleon–nucleon interaction generally in agreement. Additionally, ISM calculations [55] have predicted the $2\nu\beta\beta$ decay half-life before the experimental confirmation [56]. As such, we find ISM as the preferred method for the calculation of NME.

Section 2 presents the statistical model framework in which we conduct the study presented in this paper. We describe our methodology and explain our setup. In the last section, Section 3, we present our results for the $0\nu\beta\beta$ NME of ^{82}Se as they emerge from the Bayesian Model Averaging statistical study, together with our comments and conclusions. In previous works (see, for example, Refs. [37,38]), we performed validations of the effective Hamiltonians in the *jj*55 model space. Our work presented here elevates those studies by also performing a thorough analysis of the correlations that appear in the calculations of the observables that we compare to the experimental data in the *jj*44 model space.

2. The Statistical Model Framework

Continuing in the trend of Ref. [57] and Ref. [58] for ^{48}Ca in the *fp* model space and ^{132}Xe in the *jj55* model space, respectively, we turn our attention to the *jj44* model space, also called f_5pg_9, that is relevant for ^{76}Ge and ^{82}Se. The *jj44* model space comprises of a ^{56}Ni core and the $1p_{3/2}$, $1p_{1/2}$, $0f_{5/2}$, and $0g_{9/2}$ valence orbitals. The recipe of Ref. [58] involves the use of three starting effective Hamiltonians that are modified into sets of 1000 Hamiltonians by randomly varying the values for each of their two-body matrix elements (TBME) within $\pm$10% of their original values. The single-particle energies (SPE) are kept at their initial values. Since the calculations for ^{76}Ge are more difficult, we perform this statistical study for the decay of ^{82}Se in the same model space. No truncation of the model space is employed in this analysis, similar to our previous studies. Following the interest generated by Ref. [57], other statistical studies have been performed, such as searching for correlations between neutrinoless double-β, double Gamow–Teller, and double-magnetic decays in the pnQRPA [59], where the authors found linear correlations between $0\nu\beta\beta$ decays and both double Gamow–Teller and M1M1 transition probabilities.

In this paper, our three starting Hamiltonians are JUN45 [60], GCN:2850 [61], and JJ44b [62]. These effective Hamiltonians are obtained by starting with a theoretical Hamiltonian derived from a microscopic interaction from the Bonn-C potential that is further fitted and improved with experimental data. Ref. [60] provides a very detailed description of how JUN45 and similar effective Hamiltonians are obtained, how they differ in terms of single-particle energies and two-body matrix elements, how they deal with missing orbitals, and the Ikeda sum rule not being satisfied. In the particular case of the *jj44* model space, the ^{56}Ni core is considered "soft", leading to the yrast states in ^{57}Ni not being pure single-particle states. Thus, the single-particle energies can not simply be taken from experimental energy levels of one-hole or one-particle states over the ^{56}Ni core and need to be fitted when constructing the effective Hamiltonians.

For our study, with each modified Hamiltonian, we calculate a set of observables that enter the statistical model. These observables, besides the $0\nu\beta\beta$ NME, are: $2\nu\beta\beta$ NME, energies of the first 2^+, 4^+, and 6^+ states in ^{82}Se and ^{82}Kr, B(E2)$\uparrow$ transition probabilities of ^{82}Se and ^{82}Kr to the first 2^+ states, the Gamow–Teller transition probability from ^{82}Se and from ^{82}Kr to the 1^+ excited state in ^{82}Br. In Ref. [58], proton occupancies and neutron vacancies were also used in the analysis. For the case of ^{82}Se and ^{82}Kr, we could not identify reliable data to compare against, thus these are excluded from the present study. The correlations of the variations between pairs of these observables are carefully studied, bringing more insight into the consistency of the calculations, but also searching for non-trivial connections. This comprehensive treatment of the observables could peak interest and open a path to further developments of new effective Hamiltonians where more experimental data could be fed into the fit procedures. Seeing how these observables correlate in the calculations could prove useful for reducing the number of fit parameters and providing optimal coverage of the affected observables.

The thorough details of the calculation of these observables are found in Refs. [57,58,63]. It is worth mentioning that for the calculations of the Gamow–Teller transition probabilities and for the $2\nu\beta\beta$ NME, we use a quenching value $q = 0.74$ that is typical in the *fp* model space for ^{48}Ca with most Hamiltonians and very close to the one we use in the *jj55* model space for ^{124}Sn, ^{130}Te, and ^{136}Xe with the SVD Hamiltonian [64]. The effects of varying the quenching factor q in the statistical study of ^{136}Xe are found in Ref. [63]. For $M_{0\nu}$, we

use the closure approximation that replaces the energy of the intermediate states with an average energy, and the result is presented without quenching. The choice for the short-range correlation parametrization is Jastrow with CD-Bonn constants, which is quite soft and provides very similar results to UCOM, which is equally popular. Since we do not fine-tune any model parameters to fit the data available, we use the standard values in the case of all three starting Hamiltonians and their derived ones. While careful fine-tuning the model parameters and the interaction would improve the results for a specific case that one is interested in, the practice of over-fitting decreases the universality of the Hamiltonian, puts its prediction power into question, and most importantly, can have hidden effects on observables that were not considered in the process of fine-tuning, such as changing the shape of the nucleus or altering its magicity.

3. Results, Discussions, and Conclusions

To establish a baseline for our statistical study, we calculate the observables using the three original starting Hamiltonians and compare them to the experimental data. With this information, we can proceed to present the statistical data from our calculations using 1000 variations of each original Hamiltonian that is used in the Bayesian Model Averaging.

In Table 1, the first column presents the name of the observable, where the leading letters "**P**" and "**D**" denote the parent ^{82}Se and daughter ^{82}Kr nuclei, respectively. $M_{0\nu}$ is the $0\nu\beta\beta$ NME, $M_{2\nu}$ the $2\nu\beta\beta$ NME, GT denotes the Gamow–Teller transition probabilities to the first 1^+ state in the intermediate nucleus ^{82}Br, $BE(2)\uparrow$ are the quadupole transition probabilities to the first 2^+ state, and E_{2^+}, E_{4^+}, and E_{6^+} are the energies of the first 2^+, 4^+, and 6^+ states, respectively. Columns 2 and 3 represent the experimental data and the error. In the case of the energy levels, an error value of 150 keV was chosen, as discussed in Refs. [57,58,63]. Columns 4–6 show the values obtained using the starting Hamiltonians gcn_s, jun_s, and jun_s, followed by the average value after 1000 iterations , μ_{gcn}, μ_{jun}, μ_{gcn} and their corresponding standard deviation σ_{gcn}, σ_{jun}, and σ_{jj44}.

Reading the data in Table 1, it appears that the average values for the observables are very close to those obtained with the starting Hamiltonians and the standard deviations are reasonable, indicating no dramatic "phase-transition"-like behavior or hidden domination of the very specific TBME. We consider this a very good thing, lending credibility to the stability of the shell model calculations and their general power of prediction. One should bear in mind that despite the results being so similar between the starting Hamiltonians, they are actually quite different with differences in the order of MeV between some of their SPE for the same orbitals and also MeV differences between some of their TBME, both diagonal and off-diagonal.

Figure 1 displays a "heat map"-type plot of the Pearson correlation coefficient between pairs of observables. Also shown are the values of the Pearson coefficient ranging from 1, a perfect correlation, to -1, a perfect anti-correlation, and 0 being totally uncorrelated. We consider the variation of a pair of observables as correlated when the Pearson coefficient is above 0.5 or below -0.5. Similar to the cases of ^{48}Ca and ^{136}Xe, the variations in $M_{0\nu}$ and $M_{2\nu}$ correlate with a factor greater than 0.8, indicating a very strong correlation between these observables. This is not actually trivial, since the details of their calculation are quite different, with $M_{2\nu}$ depending on the 1^+ states in the intermediary nucleus, with $M_{0\nu}$ going through all the virtual states permitted by the neutrino momentum. Expected correlations appear among the energies of the excited states and between the 1^+ states and the $BE(2)\uparrow$ probabilities. One can notice a strong correlation between the energy levels in the parent and in the daughter nuclei, offering some confidence for future calculations for a transition involving excited states.

Table 1. The experimental data, the calculated values with the starting Hamiltonians, and the statistics for the relevant 12 observables.

Observable	Data	Error	gcn_s	jun_s	$jj4_s$	μ_{gcn}	σ_{gcn}	μ_{jun}	σ_{jun}	μ_{jj4}	σ_{jj4}
$M_{0\nu}$	N/A	N/A	2.942	3.326	2.835	2.960	0.204	3.322	0.220	2.829	0.184
$M_{2\nu}$	0.085	0.001	0.101	0.100	0.094	0.101	0.010	0.110	0.011	0.105	0.011
PGT	0.352	0.031	0.399	0.409	0.008	0.378	0.196	0.361	0.195	0.081	0.161
$PBE2$	0.252	0.008	0.133	0.130	0.143	0.131	0.005	0.129	0.007	0.141	0.006
PE_{2^+}	0.655	0.150	0.657	0.729	0.719	0.671	0.050	0.754	0.086	0.734	0.056
PE_{4^+}	1.735	0.150	1.721	1.848	2.002	1.736	0.079	1.880	0.129	2.016	0.089
PE_{6^+}	3.145	0.150	3.038	3.216	3.634	3.043	0.095	3.235	0.130	3.633	0.111
DGT	0.012	0.005	0.031	0.042	0.000	0.034	0.024	0.045	0.026	0.008	0.018
$DBE2$	0.225	0.007	0.137	0.145	0.185	0.139	0.014	0.148	0.015	0.185	0.022
DE_{2^+}	0.777	0.150	0.791	0.882	0.808	0.794	0.058	0.881	0.060	0.803	0.060
DE_{4^+}	1.821	0.150	1.807	2.001	1.939	1.810	0.108	1.989	0.113	1.928	0.131
DE_{6^+}	2.920	0.150	2.709	2.995	3.205	2.722	0.143	2.996	0.182	3.178	0.195

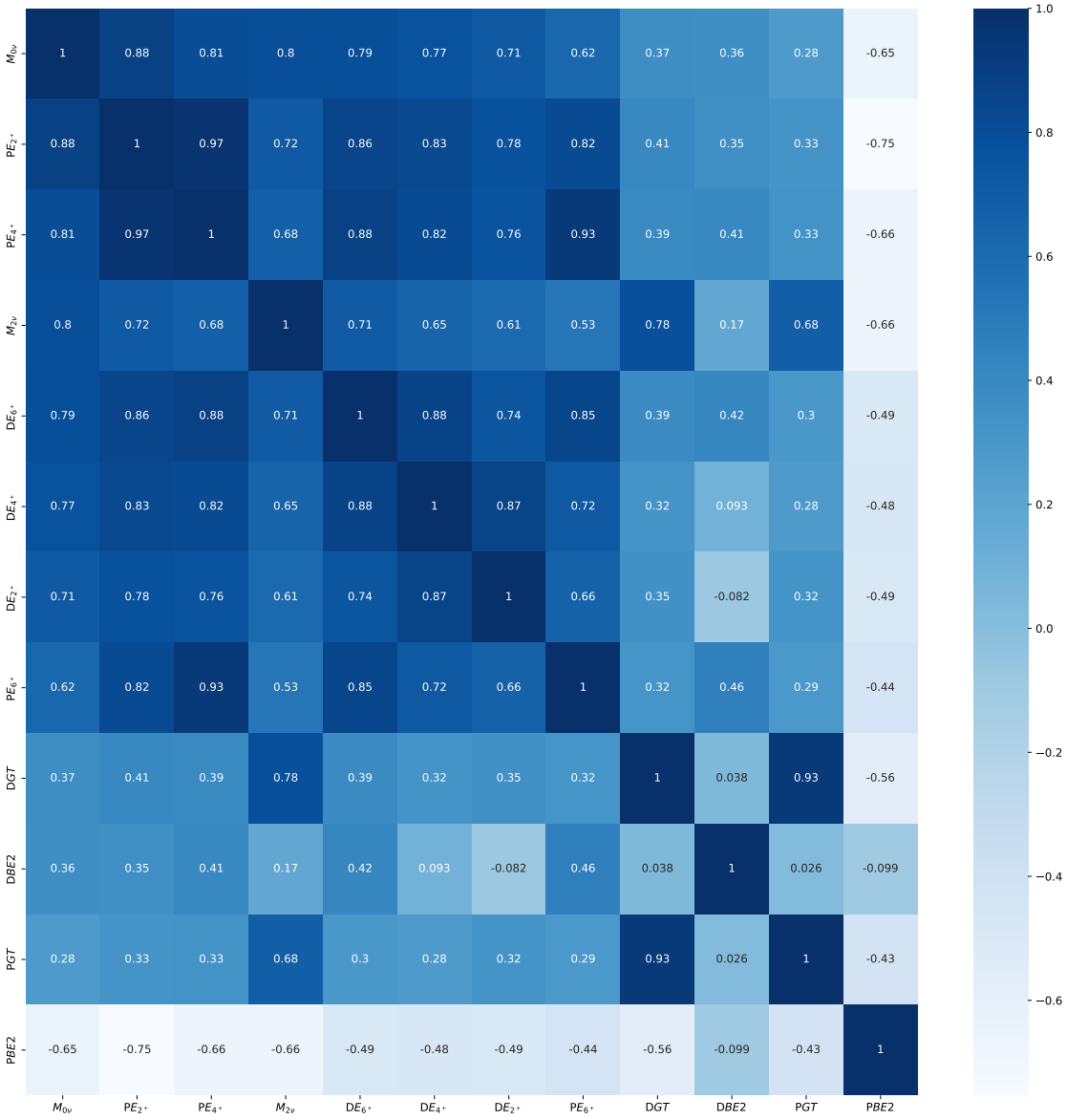

Figure 1. The heatmap for all 12 observables when using the GCN28:50 effective Hamiltonian. Very similar representations are obtained with the JUN45 and JJ44b Hamiltonians.

For the interesting cases where the absolute value of the Pearson correlation coefficient is larger than 0.5, we present the reader with an easy-to-visualize correlation matrix in Figure 2, where the contour plots show the density gradient of the calculated values and the bubble plot shows the spread of values with a dataset reduced by a factor of 10, such that it is legible. Since the diagonal would show only a straight line for the perfect correlation between an observable and itself, we utilize that space to display the histogram of that observable. For all of the observables, the distribution of the values follows a Gaussian shape, which is expected in calculations that are not strongly dependent on a specific value of a parameter.

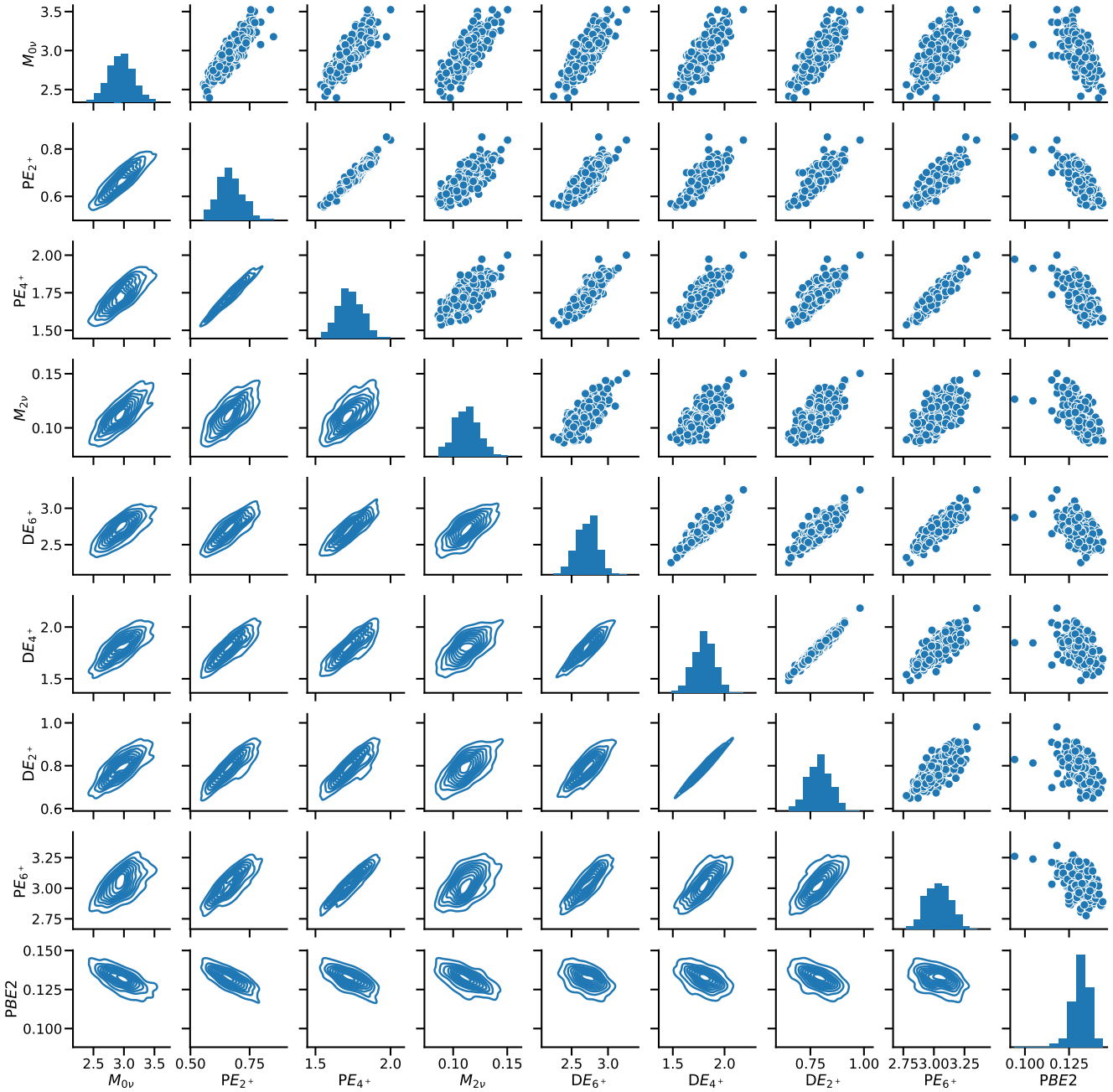

Figure 2. Correlation matrix for observables that have correlation factor greater than 0.5, when using the GCN28:50 Hamiltonian.

From a visualisation perspective, the closer the contour lines or the scattered bubbles come to a diagonal, like in Figure 2, the more correlated the pair of observables is. Very clear examples can be seen with the 4^+ and 2^+ energies of the parent and daughter, but also with the $M_{0\nu}$ and $M_{2\nu}$. Examples of anti-correlation come from the parent $BE(2)\uparrow$ and several observables where the values cluster along the other diagonal line.

Figure 3 presents, in blue bins and blue lines, the distributions for the calculated values of the 12 observables, and with red lines, the experimental data. The width of the experimental distributions corresponds to the experimental error presented in Table 1. A green vertical line with no width denotes the original values calculated with the starting Hamiltonian. Like in the case of Figures 1 and 2, for the other two types of Hamiltonians, the images are quite similar and would not provide further value to the reader.

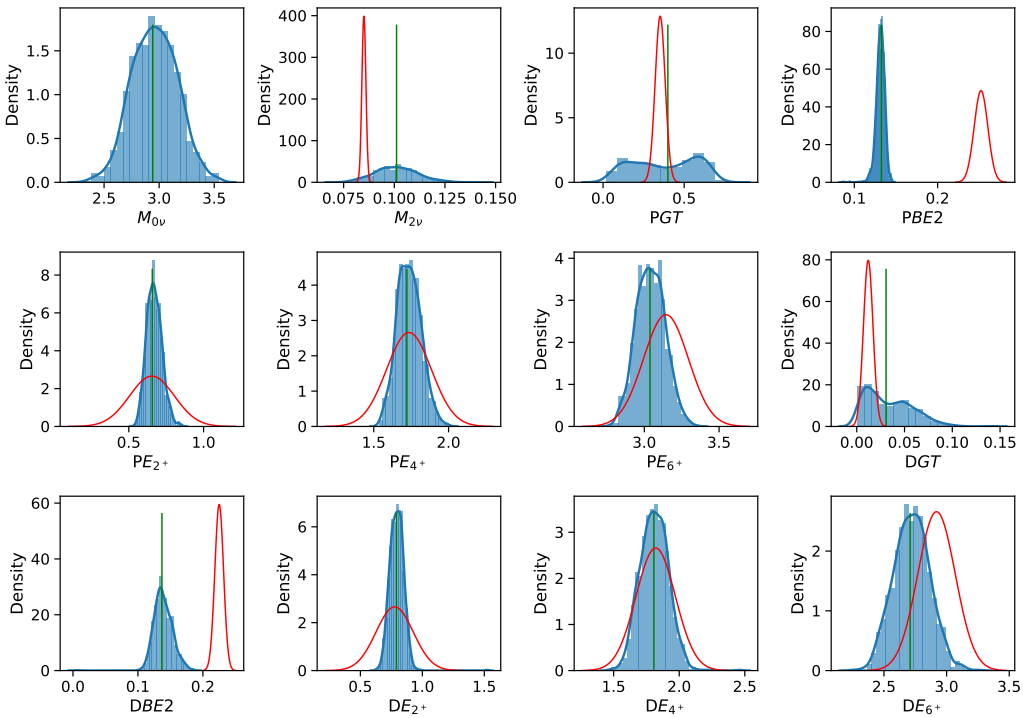

Figure 3. Distributions based on experimental data (in red) compared with the KDE (in blue) obtained from the GCN28:50 starting Hamiltonian. The green bars indicate the values of the observables for the starting effective Hamiltonians.

In the case of the JUN45 starting effective Hamiltonian, we present the calculated distributions for the 12 observables and a comparison of the experimental data in Figure 4. The obtained distributions are similar to those of GCN28:50 and JJ44b. JUN45 is fitted with different experimental data than GCN28:50, and the small impact on the 12 observables can be noted when carefully comparing the results.

In Figure 5, we show our results for the distributions of the 12 when using the JJ44b starting Hamiltonian. Again, a careful inspection reveals the small differences when compared to the other starting Hamiltonians. One more noticeable impact is on the very low values of the GT probabilities, where the changes to the TBME of the Hamiltonian can suppress the results close to 0. It is to be noted that the experimental data also show small values, and this leaves very little room for theoretical results before they fail. Just like in the case of GCN28:50 and JUN45, the $BE(2)\uparrow$ results do not overlap with the experimental value and its associated error, when calculating using the canonical charges.

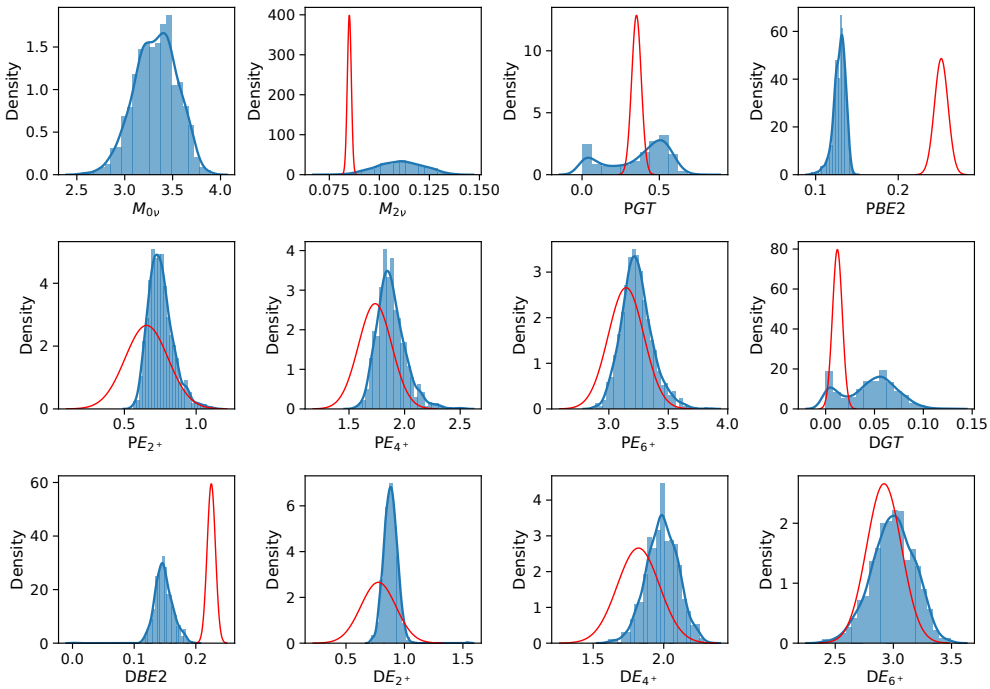

Figure 4. Similar to Figure 3, the distributions based on experimental data (in red) compared with the KDE (in blue) obtained from the JUN45 starting Hamiltonian.

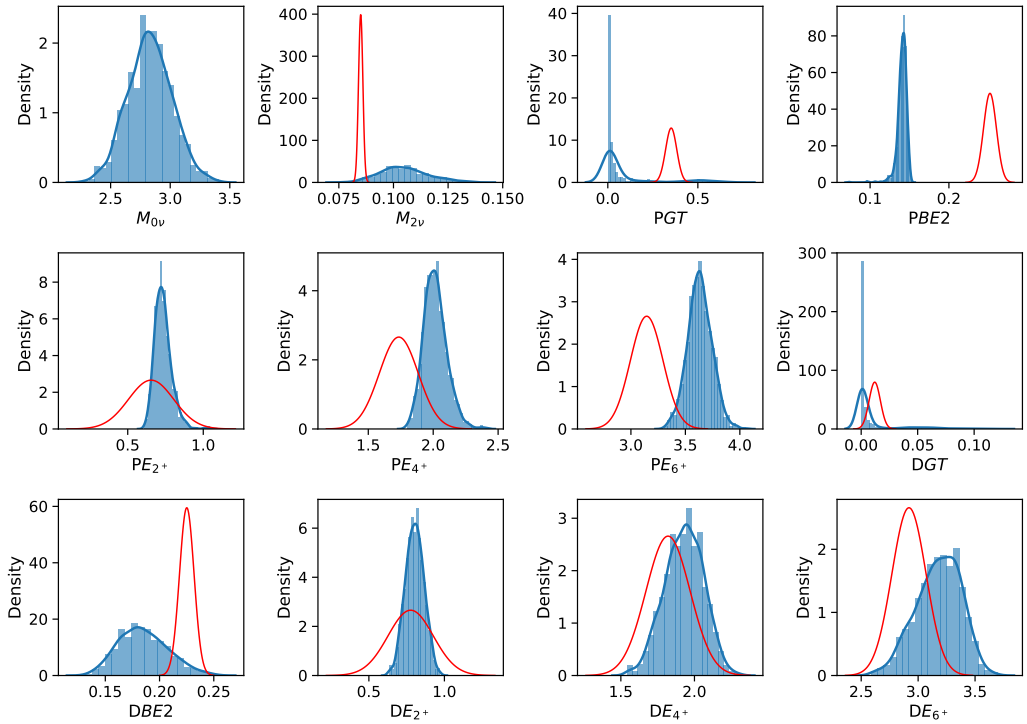

Figure 5. Similar to Figures 3 and 4, the distributions based on experimental data (in red) compared with the KDE (in blue) obtained from the JJ44b starting Hamiltonian.

The authors of Ref. [60] remark that many nuclei situated in the *jj44* model space are deformed, with large experimental values for $BE(2)\uparrow$ for transitions along low-lying states. Due to the lack of the $f(7/2)$ and $g(7/2)$ orbitals, the *jj44* model space is not sufficient enough to describe large quadrupolar collectivity [65]. In the case of the $BE(2)\uparrow$ calculations for the parent and daughter nuclei, there is a way to make the results fit the experimental data by using recommended values for the neutron and proton charges

instead of the canonical ones that we employed. That would make our results look much better, but it is outside the purpose of our study as it does not change anything in the statistical analysis in our paper. The correlations between the observables stay exactly the same, and the results and conclusions about the $0\nu\beta\beta$ NME remain the same. The authors of Ref. [60] provide the values 0.8 and 1.8 for the neutron and proton charge, respectively, but that is only relevant when the focus is on $BE(2)\uparrow$ calculations. We can confirm that this choice of effective charges works very well for all three Hamiltonians used here, not just for JUN45. For the convenience of the reader, we list the $BE(2)\uparrow$ values for the starting Hamiltonians with the modified charges as: $PBE2_{gcn_s} = 0.2127$, $PBE2_{jun_s} = 0.2075$, $PBE2_{jj4_s} = 0.2291$, and $DBE2_{gcn_s} = 0.2311$, $DBE2_{jun_s} = 0.2446$, $DBE2_{jj4_s} = 0.3099$.

Similar to Ref. [58], we performed an analysis using Bayesian model averaging, where the data from the three sets of 1000 effective Hamiltonians was fed into the calculation to provide a probability distribution of the $0\nu\beta\beta$ NME, with a mean value, a standard deviation, and a total range. The results of the Bayesian model indicate the set of weights W_H to be used for the KDE distributions P_H, where H denotes the GCN28:50, JUN45, and JJ44b starting Hamiltonians [58,63],

$$P(M_{0\nu}) = W_{GCN28:50}P_{GCN28:50}(M_{0\nu}) + W_{JUN45}P_{JUN45}(M_{0\nu}) + W_{JJ44b}P_{JJ44b}(M_{0\nu})\,. \quad (1)$$

The weights W_H were obtained using the so-called evidence integrals, Equations (4) and (5) of Ref. [58] assuming equal prior probabilities, 1/3, for all three distributions P_H. The direct result of this analysis favors the GCN28:50 staring Hamiltonian with weight 1, the others being 0. This comes mainly from the accuracy of the spectra and the fact that JJ44b provided quite poor values of the Gamow–Teller transition probabilities. However, as in Refs. [58,63], we consider for the weights W_H, an average between the prior probabilities 1/3 each and the posterior probabilities 1, 0, 0 for GCN28:50, JUN45, and JJ44b, respectively. The final weights, W_H, are 4/6 for GCN28:50, 1/6 for JUN45, and 1/6 for JJ44b. Since the values of the $0\nu\beta\beta$ NME were similar between the three sets of Hamiltonians and the GCN28:50 values sit between the JUN45 and the JJ44b ones, the the weighted sum of the $0\nu\beta\beta$ NME also resembles the GCN28:50 distribution. This makes it look like a democratic distribution of the weights despite being very influenced by the GCN28:50 results. One could infer that, unlike in other model spaces, in the $jj44$ one, the choice of effective Hamiltonian does not play a major role in the disagreement on the NME values that is still present in the literature. Previous works [37,38,66] have shown that the effects of missing spin-orbit partners can only account for about 20% of the NME value, thus not being of a major concern compared to the factor of 5 difference for ^{130}Te in Refs. [53,54].

Figure 6 presents our probability distribution function (PDF) of the $0\nu\beta\beta$ NME using results of the Bayesian model averaging analysis labeled "weighted sum", together with the PDF coming from the tree sets of Hamiltonians. The three probability distributions corresponding to each starting Hamiltonian are the kernel density estimation (KDE) obtained from the statistical sampling. They are the same distributions that appear in the upper left panel in Figures 3–5. They have been obtained using the standard data analysis Pandas package for Python, and they are properly normalized to one. The weighted sum curve in Figure 6 is a linear combination of the other three with weight normalized to unity, and therefore, this PDF is also normalized to one. In the same fashion, we calculated the mean value of the weighted sum, corresponding to the expectation value of the NME, and its standard corresponds to the error in the NME. To find a range of values for the NME at 90% confidence level, we performed numerical integration of the weighted PDF from left and right, until we reach 5% in each case. The units for the PDFs in Figure 4 are units of a density distribution that are the inverse of the units of the variable, the NME in this case, which is dimensionless. There is a significant overlap between the final result ("weighted sum") and the distributions from the individual Hamiltonians, indicating that shell model calculations provide consistent and reliable results for the $0\nu\beta\beta$ NME in the $jj44$ model space, regardless of the Hamiltonians used or any specific optimization that was

employed during the calculation. This is in contrast to calculations using other methods, as can be clearly seen in Figure 5 of Ref. [53], where the QRPA results of different groups can have very significant differences, mainly attributed to parameters such as g_{pp} that need to be adjusted for every specific calculation.

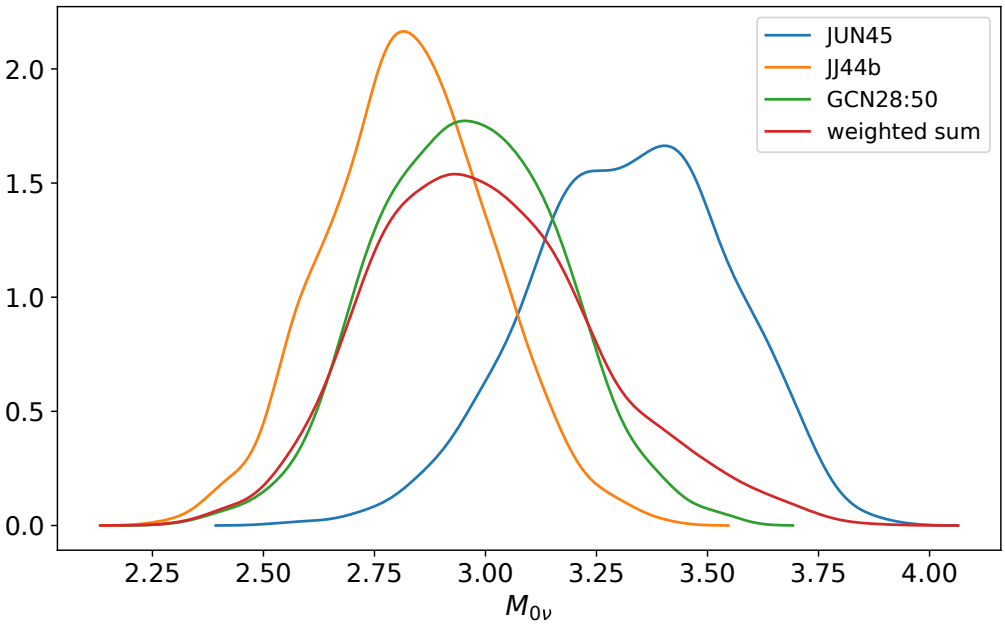

Figure 6. PDFs of the $0\nu\beta\beta$ NME distributions for the JUN45 jj44b and GCN28:50 Hamiltonians and their weighted sum (red curve, see text for details).

The weighted sum result presented in Figure 6 can now be used to provide a more realistic extraction of the experimental sensitivity to the neutrino mass. Placing a known and controlled uncertainty on the theoretical calculations would enable better predictions for the amount of expensive isotopes that are needed to expand the current experiments that can only access the inverted mass hierarchy into the next generation ones that would delve into the much lower normal mass hierarchy. This PDF can also replace the "error bars" that we sometimes plot between several points corresponding to calculations with specific choices for short-range correlation parameters, finite size effects, higher-order corrections to the nucleon currents, different effective Hamiltonians, etc.

In conclusion, we present the $0\nu\beta\beta$ NME of ^{82}Se using a shell model statistical analysis employing Bayesian model averaging, with 3000 effective Hamiltonians derived from three starting Hamiltonians (GCN28:50, JUN45, and JJ44b), providing a $0\nu\beta\beta$ NME expectation value of 3, standard deviation of 0.47, and a range of 2.55 to 3.6 at the 90% confidence level. The starting Hamiltonians were altered by randomly changing the values of their two-body matrix elements by $\pm$10%, then 12 observables were calculated, including the $0\nu\beta\beta$ NME, 11 of which were compared to the experimental data. We found the shell model results to be very resilient to the changes of the Hamiltonians within $\pm$10% and stable across a wide range of observables. A study of the correlations between the 12 observables was performed, and the results were similar for all three sets of 1000 effective Hamiltonians. The $0\nu\beta\beta$ NME and the $2\nu\beta\beta$ NME were found to correlate with a Pearson coefficient value of over 0.8, the excited energies were highly correlated, and the $BE(2)\uparrow$ transition probabilities of the first 2^+ excited state in the parent were found to anti-correlate with the $0\nu\beta\beta$ NME, the $2\nu\beta\beta$ NME, the first excited 2^+, 4^+ and 6^+ in both the parent and the daughter nuclei. One should bear in mind that the calculations of the $0\nu\beta\beta$ NME are unlike those for any other observables that we can test with experimental data, but correlations seen between the $0\nu\beta\beta$ NME and the others add confidence in the reliability of the $0\nu\beta\beta$ NME predictions. This type of analysis opens up the possibility to study other processes and observables through similar statistical analyses and to search for correlations between

calculations that were not considered here, such as the ordinary muon capture [67–69] that is also of experimental interest in MONUMENT [70], LEGEND [71], and nEXO [72].

Author Contributions: A.N. and M.H. have contributed equally to the conceptualization, software, validation, methodology, formal analisys, and writing of the work. All authors have read and agreed to the published version of the manuscript.

Funding: This research was funded by the Romanian Ministry of Research, Innovation and Digitization grant PNRR-I8/C9-CF264, Contract No. 760100/23.05.2023 and by the US Department of Energy grant DE-SC0022538 "Nuclear Astrophysics and Fundamental Symmetries".

Data Availability Statement: Dataset available on request from the authors.

Acknowledgments: The author acknowledges the fruitful discussion with S. Stoica.

Conflicts of Interest: The author declares no conflicts of interest.

Abbreviations

The following abbreviations are used in this manuscript:

BSM	Beyond the Standard Model
LNV	Lepton Number Violation
PSF	Phase Space Factors
NME	Nuclear Matrix Element(s)
DBD	Double Beta Decay
pn-QRPA	proton–neutron Quasiparticle Random Phase Approximation
IBA	Interacting Boson Approximation
TBME	Two-Body Matrix Elements
KDE	Kernel Distribution Estimate
PDF	Probability Distribution Function
JUN45 (jun)	name of nuclear effective Hamiltonian
GCN28:50 (gcn)	name of nuclear effective Hamiltonian
JJ44b (jj4)	name of nuclear effective Hamiltonian
jj44	nuclear valence space

References

1. Fukuda, Y.; Hayakawa, T.; Ichihara, E.; Inoue, K.; Ishihara, K.; Ishino, H.; Itow, Y.; Kajita, T.; Kameda, J.; Kasuga, S.; et al. Evidence for Oscillation of Atmospheric Neutrinos. *Phys. Rev. Lett.* **1998**, *81*, 1562–1567. [CrossRef]
2. Ahmad, Q.R.; Allen, R.C.; Andersen, T.C.; Anglin, J.D.; Bühler, G.; Barton, J.C.; Beier, E.W.; Bercovitch, M.; Bigu, J.; Biller, S.; et al. Measurement of the Rate of $\nu_e + d \rightarrow p + p + e^-$ Interactions Produced by ^8B Solar Neutrinos at the Sudbury Neutrino Observatory. *Phys. Rev. Lett.* **2001**, *87*, 071301. [CrossRef] [PubMed]
3. Pontecorvo, B. Mesonium and Antimesonium. *Sov. J. Exp. Theor. Phys.* **1958**, *6*, 429.
4. Pontecorvo, B. Neutrino Experiments and the Problem of Conservation of Leptonic Charge. *Sov. J. Exp. Theor. Phys.* **1968**, *26*, 984.
5. Taroni, A. Nobel Prize 2015: Kajita and McDonald. *Nat. Phys.* **2015**, *11*, 891. [CrossRef]
6. Arnquist, I.J.; Avignone, F.T.; Barabash, A.S.; Barton, C.J.; Bhimani, K.H.; Blalock, E.; Bos, B.; Busch, M.; Buuck, M.; Caldwell, T.S.; et al. Search for charge non-conservation and Pauli exclusion principle violation with the Majorana Demonstrator. *Nat. Phys.* **2024**, *20*, 1078–1083. [CrossRef]
7. Barabash, A. Precise Half-Life Values for Two-Neutrino Double-beta Decay: 2020 Review. *Universe* **2020**, *6*, 159. [CrossRef]
8. Agostini, M.; Benato, G.; Detwiler, J.A.; Menéndez, J.; Vissani, F. Toward the discovery of matter creation with neutrinoless $\beta\beta$ decay. *Rev. Mod. Phys.* **2023**, *95*, 025002. [CrossRef]
9. Schechter, J.; Valle, J.W.F. Neutrinoless double-beta decay in SU(2)XU(1) theories. *Phys. Rev. D* **1982**, *25*, 2951. [CrossRef]
10. Hirsch, M.; Kovalenko, S.; Schmidt, I. Extended Black box theorem for lepton number and flavor violating processes. *Phys. Lett. B* **2006**, *642*, 106. [CrossRef]
11. Avignone, F.T., III; Elliott, S.R.; Engel, J. Double beta decay, Majorana neutrinos, and neutrino mass. *Rev. Mod. Phys.* **2008**, *80*, 481. [CrossRef]
12. Vergados, J.D.; Ejiri, H.; Simkovic, F. Theory of neutrinoless double-beta decay. *Rep. Prog. Phys.* **2012**, *75*, 106301. [CrossRef] [PubMed]
13. Rodejohann, W. Neutrinoless double-beta decay and neutrino physics. *J. Phys. G* **2012**, *39*, 124008. [CrossRef]
14. Agostini, M.; Araujo, G.R.; Bakalyarov, A.M.; Balata, M.; Barabanov, I.; Baudis, L.; Bauer, C.; Bellotti, E.; Belogurov, S.; Bettini, A.; et al. Final Results of GERDA on the Search for Neutrinoless Double-beta Decay. *Phys. Rev. Lett.* **2020**, *125*, 252502. [CrossRef] [PubMed]

15. Arnquist, I.J.; Avignone, F.T.; Barabash, A.S.; Barton, C.J.; Barton, P.J.; Bhimani, K.H.; Blalock, E.; Bos, B.; Busch, M.; Buuck, M.; et al. Final Result of the Majorana Demonstrator's Search for Neutrinoless Double-β Decay in ^{76}Ge. *Phys. Rev. Lett.* **2023**, *130*, 062501. [CrossRef] [PubMed]
16. Anton, G.; Badhrees, I.; Barbeau, P.S.; Beck, D.; Belov, V.; Bhatta, T.; Breidenbach, M.; Brunner, T.; Cao, G.F.; Cen, W.R.; et al. Search for Neutrinoless Double-β Decay with the Complete EXO-200 Dataset. *Phys. Rev. Lett.* **2019**, *123*, 161802. [CrossRef] [PubMed]
17. Abe, S.; Asami, S.; Eizuka, M.; Futagi, S.; Gando, A.; Gando, Y.; Gima, T.; Goto, A.; Hachiya, T.; Hata, K.; et al. Search for the Majorana Nature of Neutrinos in the Inverted Mass Ordering Region with KamLAND-Zen. *Phys. Rev. Lett.* **2023**, *130*, 051801. [CrossRef] [PubMed]
18. Doi, M.; Kotani, T.; Nishiura, H.; Takasugi, E. Double beta decay. *Progr. Theor. Exp. Phys.* **1983**, *69*, 602. [CrossRef]
19. Doi, M.; Kotani, T.; Takasugi, E. Double-beta decay and Majorana neutrino. *Prog. Theor. Phys. Suppl.* **1985**, *83*, 1. [CrossRef]
20. Suhonen, J.; Civitarese, O. Weak-interaction and nuclear-structure aspects of nuclear double beta decay. *Phys. Rep.* **1998**, *300*, 123. [CrossRef]
21. Nițescu, O.; Ghinescu, S.; Sevestrean, V.A.; Horoi, M.; Šimkovic, F.; Stoica, S. Theoretical analysis and predictions for the double electron capture of ^{124}Xe. *arXiv* **2024**, arXiv:2402.13784.
22. Nițescu, O.; Ghinescu, S.; Stoica, S.; Šimkovic, F. A Systematic Study of Two-Neutrino Double Electron Capture. *Universe* **2024**, *10*, 98. [CrossRef]
23. Nițescu, O.; Dvornický, R.; Šimkovic, F. Atomic corrections for the unique first-forbidden β transition of Re187. *Phys. Rev. C* **2024**, *109*, 025501. [CrossRef]
24. Nițescu, O.; Dvornický, R.; Stoica, S.; Šimkovic, F. Angular Distributions of Emitted Electrons in the Two-Neutrino $\beta\beta$ Decay. *Universe* **2021**, *7*, 147. [CrossRef]
25. Nabi, J.U.; Ishfaq, M.; Nițescu, O.; Mirea, M.; Stoica, S. $\beta-$-Decay Half-Lives of Even-Even Nuclei Using the Recently Introduced Phase Space Recipe. *Universe* **2019**, *6*, 5. [CrossRef]
26. Mirea, M.; Pahomi, T.; Stoica, S. Phase space factors for double beta decay: An up-date. *Rom. Rep. Phys.* **2015**, *67*, 872.
27. Stoica, S.; Mirea, M. New calculations for phase space factors involved in double-beta decay. *Phys. Rev. C* **2013**, *88*, 037303. [CrossRef]
28. Kotila, J.; Iachello, F. Phase-space factors for double-beta decay. *Phys. Rev. C* **2012**, *85*, 034316. [CrossRef]
29. Caurier, E.; Poves, A.; Zuker, A.P. A full $0\hbar\omega$ description of the $2\nu\beta\beta$ decay of ^{48}Ca. *Phys. Lett. B* **1990**, *252*, 13. [CrossRef]
30. Caurier, E.; Nowacki, F.; Poves, A.; Retamosa, J. Shell Model Studies of the Double Beta Decays of ^{76}Ge, ^{82}Se, and ^{136}Xe. *Phys. Rev. Lett.* **1996**, *77*, 1954. [CrossRef]
31. Caurier, E.; Martinez-Pinedo, G.; Nowacki, F.; Poves, A.; Zuker, A.P. The shell model as a unified view of nuclear structure. *Rev. Mod. Phys.* **2005**, *77*, 427. [CrossRef]
32. Horoi, M.; Stoica, S.; Brown, B.A. Shell-model calculations of two-neutrino double-beta decay rates of ^{48}Ca with the GXPF1A interaction. *Phys. Rev. C* **2007**, *75*, 034303. [CrossRef]
33. Horoi, M.; Stoica, S. Shell model analysis of the neutrinoless double-beta decay of Ca-48. *Phys. Rev. C* **2010**, *81*, 024321. [CrossRef]
34. Horoi, M. Shell model analysis of competing contributions to the double-beta decay of Ca-48. *Phys. Rev. C* **2013**, *87*, 014320. [CrossRef]
35. Horoi, M.; Brown, B.A. Shell-Model Analysis of the Xe-136 Double Beta Decay Nuclear Matrix Elements. *Phys. Rev. Lett.* **2013**, *110*, 222502. [CrossRef]
36. Sen'kov, R.A.; Horoi, M. Accurate shell-model nuclear matrix elements for neutrinoless double-beta decay. *Phys. Rev. C* **2014**, *90*, 051301(R). [CrossRef]
37. Neacsu, A.; Horoi, M. Shell model studies of the ^{130}Te neutrinoless double-beta decay. *Phys. Rev. C* **2015**, *91*, 024309. [CrossRef]
38. Horoi, M.; Neacsu, A. Shell model predictions for ^{124}Sn double-β decay. *Phys. Rev. C* **2016**, *93*, 024308. [CrossRef]
39. Horoi, M.; Neacsu, A. Shell model study of using an effective field theory for disentangling several contributions to neutrinoless double-beta decay. *Phys. Rev. C* **2018**, *98*, 035502. [CrossRef]
40. Simkovic, F.; Pantis, G.; Vergados, J.D.; Faessler, A. Additional nucleon current contributions to neutrinoless double-beta decay. *Phys. Rev. C* **1999**, *60*, 055502. [CrossRef]
41. Stoica, S.; Klapdor-Kleingrothaus, H. Critical view on double-beta decay matrix elements within Quasi Random Phase Approximation-based methods. *Nucl. Phys. A* **2001**, *694*, 269. [CrossRef]
42. Rodin, V.; Faessler, A.; Simkovic, F.; Vogel, P. Assessment of uncertainties in QRPA 0 nu beta beta-decay nuclear matrix elements. *Nucl. Phys. A* **2006**, *766*, 107–131. [CrossRef]
43. Kortelainen, M.; Suhonen, J. Improved short-range correlations and 0 nu beta beta nuclear matrix elements of Ge-76 and Se-82. *Phys. Rev. C* **2007**, *75*, 051303(R). [CrossRef]
44. Faessler, A.; Rodin, V.; Simkovic, F. Nuclear matrix elements for neutrinoless double-beta decay and double-electron capture. *J. Phys. G* **2012**, *39*, 124006. [CrossRef]
45. Simkovic, F.; Rodin, V.; Faessler, A.; Vogel, P. $0\nu\beta\beta$ and $2\nu\beta\beta$ nuclear matrix elements, quasiparticle random-phase approximation, and isospin symmetry restoration. *Phys. Rev. C* **2013**, *87*, 045501. [CrossRef]
46. Barea, J.; Iachello, F. Neutrinoless double-beta decay in the microscopic interacting boson model. *Phys. Rev. C* **2009**, *79*, 044301. [CrossRef]
47. Barea, J.; Kotila, J.; Iachello, F. Nuclear matrix elements for double-beta decay. *Phys. Rev. C* **2013**, *87*, 014315. [CrossRef]

48. Rodriguez, T.R.; Martinez-Pinedo, G. Energy Density Functional Study of Nuclear Matrix Elements for Neutrinoless beta beta Decay. *Phys. Rev. Lett.* **2010**, *105*, 252503. [CrossRef] [PubMed]
49. Rath, P.K.; Chandra, R.; Chaturvedi, K.; Lohani, P.; Raina, P.K.; Hirsch, J.G. Neutrinoless beta beta decay transition matrix elements within mechanisms involving light Majorana neutrinos, classical Majorons, and sterile neutrinos. *Phys. Rev. C* **2013**, *88*, 064322. [CrossRef]
50. Novario, S.; Gysbers, P.; Engel, J.; Hagen, G.; Jansen, G.R.; Morris, T.D.; Navrátil, P.; Papenbrock, T.; Quaglioni, S. Coupled-Cluster Calculations of Neutrinoless Double-β Decay in ^{48}Ca. *Phys. Rev. Lett.* **2021**, *126*, 182502. [CrossRef]
51. Yao, J.M.; Bally, B.; Engel, J.; Wirth, R.; Rodríguez, T.R.; Hergert, H. Ab Initio Treatment of Collective Correlations and the Neutrinoless Double Beta Decay of ^{48}Ca. *Phys. Rev. Lett.* **2020**, *124*, 232501. [CrossRef]
52. Belley, A.; Payne, C.G.; Stroberg, S.R.; Miyagi, T.; Holt, J.D. Ab Initio Neutrinoless Double-Beta Decay Matrix Elements for ^{48}Ca, ^{76}Ge, and ^{82}Se. *Phys. Rev. Lett.* **2021**, *126*, 042502. [CrossRef] [PubMed]
53. Engel, J.; Menéndez, J. Status and future of nuclear matrix elements for neutrinoless double-beta decay: A review. *Rep. Prog. Phys.* **2017**, *80*, 046301. [CrossRef] [PubMed]
54. Dolinski, M.J.; Poon, A.W.; Rodejohann, W. Neutrinoless Double-Beta Decay: Status and Prospects. *Annu. Rev. Nucl. Part. Sci.* **2019**, *69*, 219–251. [CrossRef]
55. Retamosa, J.; Caurier, E.; Nowacki, F. Neutrinoless double beta decay of ^{48}Ca. *Phys. Rev. C* **1995**, *51*, 371. [CrossRef] [PubMed]
56. Balysh, A.; DeSilva, A.; Lebedev, V.I.; Lou, K.; Moe, M.K.; Nelson, M.A.; Piepke, A.; Pronskiy, A.; Vient, M.A.; Vogel, P. Double beta decay of Ca-48. *Phys. Rev. Lett.* **1996**, *77*, 5186. [CrossRef] [PubMed]
57. Horoi, M.; Neacsu, A.; Stoica, S. Statistical analysis for the neutrinoless double-β-decay matrix element of ^{48}Ca. *Phys. Rev. C* **2022**, *106*, 054302. [CrossRef]
58. Horoi, M.; Neacsu, A.; Stoica, S. Predicting the neutrinoless double-β-decay matrix element of ^{136}Xe using a statistical approach. *Phys. Rev. C* **2023**, *107*, 045501. [CrossRef]
59. Jokiniemi, L.; Menéndez, J. Correlations between neutrinoless double-β, double Gamow-Teller, and double-magnetic decays in the proton-neutron quasiparticle random-phase approximation framework. *Phys. Rev. C* **2023**, *107*, 044316. [CrossRef]
60. Honma, M.; Otsuka, T.; Mizusaki, T.; Hjorth-Jensen, M. New effective interaction for f_5pg_9-shell nuclei. *Phys. Rev. C* **2009**, *80*, 064323. [CrossRef]
61. Menéndez, J.; Poves, A.; Caurier, E.; Nowacki, F. Disassembling the nuclear matrix elements of the neutrinoless $\beta\beta$ decay. *Nucl. Phys. A* **2009**, *818*, 139–151. [CrossRef]
62. Cheal, B.; Mané, E.; Billowes, J.; Bissell, M.L.; Blaum, K.; Brown, B.A.; Charlwood, F.C.; Flanagan, K.T.; Forest, D.H.; Geppert, C.; et al. Nuclear Spins and Moments of Ga Isotopes Reveal Sudden Structural Changes between $N = 40$ and $N = 50$. *Phys. Rev. Lett.* **2010**, *104*, 252502. [CrossRef] [PubMed]
63. Horoi, M. Improved Statistical Analysis for the Neutrinoless Double-Beta Decay Matrix Element of ^{136}Xe. *Universe* **2024**, *10*, 252. [CrossRef]
64. Qi, C.; Xu, Z.X. Monopole-optimized effective interaction for tin isotopes. *Phys. Rev. C* **2012**, *86*, 044323. [CrossRef]
65. Zuker, A.P.; Retamosa, J.; Poves, A.; Caurier, E. Spherical shell model description of rotational motion. *Phys. Rev. C* **1995**, *52*, R1741–R1745. [CrossRef]
66. Sen'kov, R.A.; Horoi, M.; Brown, B.A. Neutrinoless double-beta decay of Se-82 in the shell model: Beyond the closure approximation. *Phys. Rev. C* **2014**, *89*, 054304. [CrossRef]
67. Kortelainen, M.; Suhonen, J. Ordinary muon capture as a probe of virtual transitions of double-beta decay. *Europhys. Lett.* **2002**, *58*, 666. [CrossRef]
68. Kortelainen, M.; Suhonen, J. Microscopic study of muon-capture transitions in nuclei involved in double-beta-decay processes. *Nucl. Phys. A* **2003**, *713*, 501–521. [CrossRef]
69. Zinatulina, D.; Brudanin, V.; Egorov, V.; Petitjean, C.; Shirchenko, M.; Suhonen, J.; Yutlandov, I. Ordinary muon capture studies for the matrix elements in $\beta\beta$ decay. *Phys. Rev. C* **2019**, *99*, 024327. [CrossRef]
70. Bajpai, D.; Baudis, L.; Belov, V.; Bossio, E.; Cocolios, T.E.; Ejiri, H.; Sushenok, E.; Fomina, M.; Hashim, I.H.; Heines, M.; et al. The MONUMENT Experiment: Ordinary Muon Capture studies for neutrinoless double-beta decay. *arXiv* **2024**, arXiv:2404.12686.
71. Collaboration, L.; Abgrall, N.; Abt, I.; Agostini, M.; Alexander, A.; Andreoiu, C.; Araujo, G.R.; Avignone, F.T., III; Bae, W.; Bakalyarov, A.; et al. LEGEND-1000 Preconceptual Design Report. *arXiv* **2021**, arXiv:2107.11462.
72. Adhikari, G.; Kharusi, S.A.; Angelico, E.; Anton, G.; Arnquist, I.J.; Badhrees, I.; Bane, J.; Belov, V.; Bernard, E.P.; Bhatta, T.; et al. nEXO: Neutrinoless double beta decay search beyond 1028 year half-life sensitivity. *J. Phys. G Nucl. Part. Phys.* **2021**, *49*, 015104. [CrossRef]